Published in final edited form as:
*Top Magn Reson Imaging*. 2010 December ; 21(6): 355–365. doi:10.1097/RMR.0b013e31823f6413.

# Challenges of High Resolution Diffusion Imaging of the Human Medial Temporal Lobe in Alzheimer's Disease

**Michael M. Zeineh, M.D.-Ph.D.**,
Stanford University

**Samantha Holdsworth, Ph.D.**,
Stanford University

**Stefan Skare, Ph.D.**,
Karolinska Institutet

**Scott W. Atlas, M.D.**, and
Stanford University

**Roland Bammer, Ph.D**
Stanford University

## Abstract

The human medial temporal lobe performs an essential role in memory formation and retrieval. Diseases involving the hippocampus such as Alzheimer's disease present a unique opportunity for advanced imaging techniques to detect abnormalities at an early stage. In particular, it is possible that diffusion imaging may measure abnormal microarchitecture beyond the realm of macroscopic imaging. However, this task is formidable because of the detailed anatomy of the medial temporal lobe, the difficulties in obtaining high quality diffusion images of adequate resolution, and challenges in diffusion data processing. Moreover, it is unclear if any differences will be significant for an individual patient or simply groups of patients. Successful endeavors will need to address each of these challenges in an integrated fashion. The rewards of such analysis may be detection of microscopic disease *in vivo*, which could represent a landmark accomplishment for the field of neuroradiology.

### Keywords

Diffusion; Tractography; Hippocampus; Alzheimer's

## Introduction

The overall aim of this paper is to discuss the application of diffusion tensor imaging (DTI) to the medial temporal lobe, with particular attention to interrogating abnormalities in Alzheimer's disease (AD). We provide in-depth description of the underlying neuroanatomy and relevant neuropathology in AD, and we review some of the impressive clinical DTI studies done to-date. Following a detailed discussion on the limitations and challenges of current implementations of DTI, we provide some recommendations for improving the image quality and reproducibility for future scientific studies as well as clinical applications.

Correspondence Address: Michael M. Zeineh Stanford University 300 Pasteur Dr., Rm S-047 Stanford, CA, 94305-5105 t: 650-721-1419 f: 650-498-5374 mzeineh@satnford.edu.

The same techniques and concepts described here also apply to diseases such as mesial temporal sclerosis and other degenerative disorders of the temporal lobe.

## A Brief History of Studies of Medial Temporal Lobe Function

An Italian anatomist named Julius Caesar Arantius was the first to name and describe the hippocampus in 1587 [1, 2]. The term translates as “horse-caterpillar.” While in Greek and Roman mythology *hippocampus* refers to a marine god sitting atop a seahorse, it is believed Arantius meant the small sea creature. He also applied the name *bombycinus vermis*, Latin for silkworm, though this was not his preferred name for the structure. A complicated history of medial temporal lobe terminology ensued. The term hippocampus still stands, but several other terms have been adopted such as *pez hippocampi* and *Ammon's horn*, which now have specific references to micro-anatomy, though not necessarily consistent with their historical derivation.

For some time, the hippocampus was thought to be primarily important for olfactory processing. In a 1937 paper, Papez (pronounced pāpes) tabulated some of the known clinical conditions affecting the hippocampus, cingulum, mammillary bodies, and anterior thalamus. For example, he noted that rabies was known to affect the hippocampus and result in “emotional perturbation.” [3] He theorized that these structures were critical for emotional processing, and together they have become known as the circuit of Papez. It was not until the 1950s with studies of patient Henry Gustav Molaison, known while he was alive as H.M., that the nature of hippocampal function became known. H.M. underwent bilateral medial temporal lobectomy for epilepsy and subsequently developed profound and permanent anterograde amnesia [4, 5]. In the past forty years, extensive work has been conducted studying the neural substrate of memory, focusing on the hippocampus and surrounding structures, collectively termed the medial temporal lobe (MTL). These inquiries have utilized a spectrum of investigative techniques including electrophysiology, animal and human lesion studies, molecular biology, neurochemistry, neural modeling, and various forms of brain imaging in humans and animals -- all with the goal of elucidating how the MTL functions intrinsically and interacts with the rest of the brain to carry out mnemonic function. A central theme uniting all of these studies is that memory formation requires neuronal networks developing and strengthening their interconnections to form associations [6]. The hippocampus, the centerpiece of the MTL, is the most important component of the networks underlying learning and long-term consolidation of information.

## Neuroanatomy: Hippocampal Subfields and Connectivity

From an imaging perspective, the medial temporal lobe is a unique part of the brain for many reasons. First, the complexities of its anatomy are readily apparent on modern MR structural imaging. Second, these complexities are largely consistent across subjects, barring differences in brain size and relatively minor differences in hippocampal development. Finally, the hippocampus has the distinction that its only known role is memory formation, which is crucial to normal cognitive function. This is in contradistinction to structures such as 1) the cerebellar hemispheres, which have intricate structure relatively consistent across subjects, but are not essential to cognition, 2) the thalamus, which is important to cognition and the sensorium, in which intricate structure is not apparent on conventional imaging, though its appearance is consistent across subjects, and 3) the neocortex, which is essential for language and memory among other eloquent functions, but has relatively homogeneous gross structure that varies significantly across subjects. Hence, a detailed understanding of hippocampal gross and microanatomy is beneficial for a discussion of connectivity. Additionally, alterations in anatomy and connectivity may be easier to discern from intersubject variance because of the relatively consistent anatomy.

The medial temporal lobe is a compact structure with several components (Figure 1). It can be roughly divided into two parts: the hippocampus proper and adjacent neocortical areas. The nearby cortical areas project to the hippocampus proper, and the hippocampus proper has an internal system of projections that sends output back to the nearby cortical areas [7, 8]. The details of connectivity are derived from tracer studies on the macaque monkey, whose brain has a direct anatomical correspondence with the human brain [9].

The entorhinal cortex (ERC), which lies in the anterior portion of the parahippocampal gyrus and borders the anterior hippocampus, is the main gateway of input to and output from the hippocampus proper [10]. It receives most of its projections from two adjacent areas: the perirhinal cortex (PRC) and the parahippocampal cortex (PHC). Besides the perirhinal and parahippocampal contributions, the entorhinal cortex receives input from polymodal cingulate/retrosplenial cortex, dorsal superior temporal sulcus, orbitofrontal cortex, the olfactory bulb, and parainsular cortex. Both perirhinal and parahippocampal cortices receive widespread projections from many cerebral areas.

The essential circuit diagram of the hippocampus proper is a loop (Figure 2). The main circuit starts with cells in layer II and VI of the entorhinal cortex projecting via a white matter tract called the angular bundle to innervate primarily the dentate gyrus and CA3 [11]. This comprises the perforant path, labeled as such because fibers perforate the subiculum on the way to the dentate gyrus. From the dentate gyrus, neurons synapse successively to fields CA 3 (Cornu Ammonis 3), CA 1, the subiculum, and back to layer V of the entorhinal cortex, where output returns to the parahippocampal and perirhinal cortices. A complementary projection from entorhinal layers III and V targets primarily the distal half of this circuity loop, namely CA 1 and the subiculum.

Extensive interconnections are present within the dentate and CA 3 fields. The hippocampus also interacts with subcortical structures: an output detour is taken from CA 3, the subiculum, and entorhinal cortex, via the fornix, a white matter tract that attaches to the inferior border of the septum pellucidum and synapses with the mammillary nuclei within the hypothalamus as well as the septal nuclei.

These are the most basic of pathways, and there are numerous other connections at each stage that are beyond the scope of this article. A limitation in this model is that it is almost entirely derived from animal work, with only minimal tracing studies done on human specimens, which suggested the alvear pathway may be more important in humans than in monkeys [12, 13].

It is particularly important to note the scale of the images in Figure 1. The entirety of the hippocampus and adjacent substructures lies within a span of approximately 2-2.5 cm superoinferiorly, the height of the hippocampus proper including the subiculum is only approximately 6-8 mm, and the height of CA 1 is only about 1.5mm.

## Alzheimer's and the Medial Temporal Lobe

Intensive investigations have sought to define the relationship between hippocampal dysfunction and AD, in which impaired memory formation is a distinguishing feature. Beginning in the medial temporal lobe, a complex and incompletely understood interplay of intracellular neurofibrillary tangles and extracellular amyloid plaques likely contributes to synaptic and neural degeneration [14, 15, 16, 17, 18]. By the time a clinical diagnosis is possible, there has been extensive neuronal destruction [18], and not surprisingly, there is no effective treatment for the disease. Because any effective prevention or treatment will need to occur before this neuronal loss, there is a great need for preclinical diagnosis of patients who will develop AD. Some of the well-studied methods attempting preclinical detection

include structural magnetic resonance imaging (MRI) [19, 20], functional MRI [21, 22], resting state fMRI [23], diffusion tensor MRI (DTI) [24], cerebral spinal fluid (CSF) biomarkers [25], and fluoro-deoxy glucose-PET [22]. However, all of these are indirect measures of AD pathology and are typically significant at the group level, often with limited specificity and sensitivity. There remains a need for more accurate non-invasive pre-clinical imaging. More recent developments include the tracer Pittsburgh compound B (PIB), a PET tracer that binds amyloid [26]. Unfortunately, PIB is not specific to the subtype of amyloid, and in addition to amyloid plaques associated with AD, PIB is positive for amyloid angiopathy, which is common in the elderly and not strongly associated with AD [27].

Given the current theory that long-term memory requires neural connectivity centered in the medial temporal lobe, and given that memory formation is impaired in AD, measurements of connectivity may quantitatively ascertain mnemonic capability and the relevant impairment in diseases of the MTL such as AD. Neuropathologic data suggests that cell loss in the entorhinal cortex is marked in AD, particularly at early stages, concordant with neurofibrillary tangle pathology, which is known to start in the entorhinal cortex [28, 29, 30]. Thus, DTI is uniquely poised to measure the neuronal loss in the medial temporal lobe. Tractography is a form of diffusion tensor processing that attempts to identify tracts corresponding to white matter fascicles, and it may demonstrate some promise for AD.

This paper will explore the challenges involved in using DTI of the MTL with suggestions for more consistent and sensitive research and clinical studies. This is of interest in the field of neuroradiology where there are no specific findings of Alzheimer's disease, especially at an early stage.

## The Role of Diffusion Tensor Imaging (DTI) in AD

The axonal destruction associated with neurofibrillary (i.e. plaque and tangle) pathology may be measurable by DTI. Diffusion-weighted imaging is sensitive to both the direction and magnitude of proton diffusion. In white matter, diffusion progresses primarily along the path of the axon, resulting in anisotropy in the pattern of diffusion. This is typically quantified as the fractional anisotropy (FA), a measure of how strong the diffusion is along the leading diffusion direction. The main contribution to this anisotropy is the orientation of the axons within the volume of a pixel [31]. Hence, axonal degeneration secondary to neurofibrillary-driven neural degeneration should be evident in quantitative diffusion-weighted imaging.

Many of the landmark diffusion studies in the literature demonstrate that some portion of the medial temporal lobe exhibits abnormal diffusion characteristics in AD and/or MCI patients compared to normal controls [32, 33, 34, 35, 36, 37, 38, 39, 40, 41, 42]. Similar but more minor changes are noted in mild cognitive impairment, a pre-clinical state that progresses to AD at a rate of about 10-15% a year. Two literature reviews and one meta-analysis more exhaustively summarize the results [33, 43, 44]. However, these alterations are minor among larger study groups and would not translate into useful thresholds on the single-subject level.

A detailed examination of the applied methodology finds significant variation in acquisition, processing, and in the exact location and type of result, summarized in Table 1. Perhaps one of the biggest contributors to the inconsistencies in these studies is the technical hurdles associated with the diffusion image acquisition and processing. Many of the challenges associated with performing DTI and subsequent tractography is described in detail below.

## Summary of DTI studies of the MTL in AD

**Acquisition Challenges—**Teasing apart at least some of the microstructure of the MTL, such as the perforant pathway, requires high-resolution diffusion-tensor imaging. However, even typical diffusion tensor imaging is fraught with both acquisition and processing challenges under common circumstances [45, 46], and many of these problems are exacerbated in the medial temporal lobe.

A number of methods that can be used to acquire the DTI data; echo-planar imaging (EPI) is typically used for its speed and relative insensitivity to motion. However, EPI is subject to numerous types of artifact including susceptibility distortions and signal loss. These distortions typically occur where the magnetic field is inhomogeneous, such as at air-tissue interfaces. With regard to the medial temporal lobe, the petrous apices, which are often pneumatized, can be a markedly significant source of this artifact. For EPI in any orientation, it is useful to perform parallel imaging along the phase-encode direction, as the slow bandwidth along this direction causes severe image distortion. Parallel imaging techniques, such as SENSitivity Encoding (SENSE) or Generalized Autocalibrating Partial Parallel Acquisition (GRAPPA) is known to significantly reduce distortions near the MTL. However, only three studies of the MTL in AD reviewed here have utilized parallel imaging (Table 1).

Typical structural imaging of the medial temporal lobe employs the coronal plane or even oblique coronal plane perpendicular to the long axis of the hippocampus; the slab is typically 2-3 mm thick to improve the signal to noise ratio (SNR), but generally a high in-plane resolution is employed to maximize differences in the microanatomy. However, for diffusion EPI, the typical arrangement of coils in a multichannel receive array does not facilitate parallel acceleration in the coronal plane with the phase encode direction supero-inferiorly and requires the phase encode direction to be along the left-right axis (acceleration factor 2, Figure 3). Since EPI artifacts are severe along the lower bandwidth phase-encode axis, this results in asymmetric left-right distortion with a coronal plane acquisition using parallel imaging. With EPI in any orientation, the pattern of distortion will change depending on how the phase encoding axis is traversed; this is particularly difficult in the coronal plane (Figure 4A-B) [47]. Such asymmetries could surely confound quantitative analyses of connectivity. Distortion correction methods (Figure 4c) can to some extent compensate for this but are neither widely available nor tested, and may induce a degree of blurring. Finally, there is variable pneumatization of the adjacent petrous apices that causes a significant and possibly asymmetric degree of susceptibility-based distortion of the temporal lobes (Figure 5B), which will be asymmetric in any coronal plane acquisition regardless of the phase-encode axis chosen.

The axial plane alleviates some of these asymmetries because with typical coil arrangements the phase-encode axis can be antero-posterior, preserving left-right symmetry while still allowing for parallel imaging (Figure 6). The typical slice thickness of 2-2.2mm is adequate for discerning hippocampus from adjacent substructures, but is insufficient to visualize intrahippocampal microstructure. Making slices thinner and voxels isotropic will quickly deplete the SNR to the point that noise dominates the results. For these reasons, the selection of slice thickness in the literature has varied from 2 to 5 mm (more often the latter), with the in-plane resolution varying from 1.8 mm to 3 mm. Anisotropic voxels that are small along two but not all three axes will preserve SNR, but this will result in bias in tractography and is generally avoided [45].

The coil arrangement poses a particular challenge. Newer multi-channel receiver arrays have the best SNR at the cortical surface. Volume coils have their best SNR at the center of the

brain. The hippocampi are approximately halfway between the cortex and center of the brain, making any particular coil arrangement difficult to optimize.

With regard to acquisition methodology, many reported studies have been done at 1.5 T, which offers inferior signal-to-noise ratio (SNR) to 3.0T, though the newer studies are more often at 3.0T. The SNR available even at 3.0T creates a limit on the resolution that can be achieved in clinical scanning times. Going to 7.0 Tesla has theoretical promise, but the tissue T2 and even more so the tissue T2* shorten as field strength increases, reducing the gain in SNR. Additionally, B1 inhomogeneity often results in asymmetric signal intensity within the temporal lobes. Methods are underway to improve visualization with 7T [48].

High-order shimming is known to improve B0 homogeneity in the temporal lobes with echo-planar imaging, and is available on clinical scanners [49]. The studies reported here did not describe the use of this procedure.

Microstructural interrogation requires extremely high fidelity input imaging, and the typical diffusion-weighted imaging artifacts constitute a significant impediment. The addition of diffusion gradients results in eddy current artifacts as well as longer echo times with resulting low SNR. Compensating for eddy currents with a twice-refocused diffusion preparation scheme [50] results in an increase in TE that further lowers the SNR; yet, adequate eddy current compensation is essential (Figure 7). An alternative to twice-refocusing is post-processing techniques [51], [52] [53]. However, only half of the studies reviewed here attempt to compensate for eddy currents using either of these correction approaches.

Patient motion is an additional factor that reduces data quality. While approximately half of the studies reviewed here address issues in motion, only one study corrects for motion while adjusting the b-matrix, something that is known to improve accuracy and consistency [46]. Despite these attempts at motion correction, the registration of all diffusion timepoints with the B=0 images is difficult to obtain on the fine scale required for determination of microstructure.

Crossing fibers present an additional severe challenge for two reasons. First, the perforant pathway neurons cross a major white matter pathway, the cingulum bundle, which lies within the parahippocampal gyrus. Second, the perforant path crosses the subiculum to reach the dentate gyrus and remainder of the hippocampus; the gray matter of the subiculum may restrict diffusion due to its own internal structure, further confounding the analysis. Several methods exist to address crossing fibers [54, 55, 56, 57, 58, 59, 60], but these generally require a high b-values, which starve the SNR (Figure 8), and a large number of diffusion directions, which results in prohibitively long imaging times. To combat this SNR loss, larger voxel sizes are typically employed, which again will be inadequate for microanatomy.

It is clear that the interplay of a wide variety of imaging parameters can have a significant effect on the SNR, resolution, distortion, etc. The need to trade-off between these measures of image quality explains the great variance in the parameters selected in the literature. B-values range from 700 to 1200. The number of diffusion directions was most often six, which is suboptimal for measurement of FA and MD [61], but in one study sixty directions were acquired. All acquisitions were in the axial plane, but some were obliqued to the AC-PC line. Two studies use FLAIR for CSF suppression, and one study replaces a b = 0 sec/mm$^2$ image for a b = 33 sec/mm$^2$ image without going into further details. Unfortunately, no single study employs parallel imaging, eddy current compensation, motion correction, and b-matrix adjustment all together – all of which are validated to improve image quality.

**Processing Issues—**Diffusion image processing is hampered by numerous sources of rampant variability, including region of interest selection and methodological differences in generating and quantifying tracts.

Region of interest (ROI) selection dominates the methods of quantitative DTI processing, but the exact method of defining and even naming the ROI varies from study to study, although the studies generally employ methods to assure internal consistency. ROI analyses are best when there is extensive detail with regard to the segmentation criteria [40]. Inter-rater reliability measurements provide for internal consistency [39]. Unfortunately, all of the listed studies used very different segmentation procedures and criteria. Additionally, if the segmentation procedure is not done on the b=0 image, which is often the case, then the registration between the diffusion image and the structural image needs to be exact, and this requires at least a 9 parameter affine model to coregister the two. Ideally, segmentation should be performed or verified on the b=0 image for each subject. Additionally, there are relatively standardized references for determining the subregions of the MTL [9], which can be the source of seed points for tractography.

Several studies go as far to distinguish hippocampal from parahippocampal ROIs, but with a slice thickness of 5 mm, the entire hippocampus fills a 5 mm voxel, and such distinction should be taken with caution [36, 38, 39]. A few studies use the term entorhinal cortex [37, 62], but a measurement of cortical fractional anisotropy unbiased by adjacent white matter is well beyond the resolution of any of the cited studies. Similarly, the fornix is 2-4 mm in cross section and would likely be subject to significant partial voluming effects [63]. These effects could statistically interact with patient category if there is generalized volume loss, which is the case in AD, even with FLAIR technique, which does not always result in complete CSF suppression. Two studies employed voxel-based analyses [32, 37]; this should be more objective and reproducible, but would be more difficult to translate to clinical utility, and assumes accurate registration, which is often difficult to quantify. Two studies performed tractography on the cingulum bundle within the parahippocampal gyrus, and then measured FA and/or mean diffusivity (MD) along the track [35, 40]. This is an interesting form of analysis that isolates the track of interest, though its utility is complicated by crossing fibers in the same voxel that will contribute to the measured FA or MD.

**Interpretation Challenges—**When the bilateral hippocampi and parahippocampal structures are taken together as the MTL, most studies reported a significant difference in the MTL between AD and normal controls. This interpretation is complicated by the fact that some studies interpreted the hemispheres separately, and others combined. Two studies reported significant results only for the left MTL. In most studies, results were significant for both FA and MD. However, in one study, results were significant for FA but not for MD [41], and in another study vice-versa [40]. The reason for this is unknown. One of the listed studies revealed no MTL difference except for in the fornix [63]. This is for unclear reasons, and perhaps the somewhat low b-value of 700 sec/mm$^2$ coupled with a b=33 sec/mm$^2$ rather than b=0 sec/mm$^2$ image may be a factor. Alternatively, this study only evaluated MD, and perhaps a measurement of FA would have proved significant.

## Non Alzheimer MTL Diffusion Studies

**In vivo—**An alternative acquisition scheme called Zoom-EPI has been applied in epilepsy to investigate the MTL [64]. Tilting the 180-degree refocusing pulse results in a reduced field of view along one axis because it only partially intersects the 90-degree excitation slice. By choosing this axis as the phase encode axis, the number of phase encode lines can be reduced, shortening the EPI readout, resulting in reduced distortions. The TE also shortens, offering a SNR gain, but this is offset by a SNR penalty from encoding fewer lines

of k-space. In the coronal plane, this can be used to achieve high in-plane resolution, and distortion will be left-right symmetric with the phase encode axis supero-inferiorly. In this 1.5T study, voxel size was 1.4 × 1.4 × 5mm, facilitating detailed visualization of MTL anatomy, though there was a 10mm slice gap. A Zoom-EPI image from our own implementation of the imaging sequence is demonstrated in Figure 5A. As is apparent, distortion is symmetric but still significant. Parallel imaging within slice cannot be added because typical head coil sensitivities will not be orthogonal enough along the shortened supero-inferior phase-encode axis. Other inherent limitations to the Zoom technique include slice thickness, such that it may be difficult to extend the technique to isotropic voxels because the oblique pulse will interact with adjacent slices, as well as SNR reduction at the edges of the reduced field of view (due to the reduced effective slice thickness in these regions).

Another example of coronal plane DTI is a recent novel study examining the difference between younger and older individuals [65]. Here, the voxel size was 0.66 × 0.66 × 4mm slices, with very high in-plane resolution. However, the voxels are anisotropic by a factor of 6, which could result in significant bias in tractography. The investigators thus chose an anatomy-driven definition of the perforant pathway, and took the dot product of the expected pathway with the diffusion tensor, showing subtle differences between younger and older individuals. The study did employ parallel imaging, but did not specify the phase-encode axis. Likely, the phase-encode axis was left-right given the 8-channel head coil, and asymmetric distortion was necessarily present. This asymmetric distortion is an additional source of variance that can reduce sensitivity to significant findings in AD, especially since the diffusion literature suggests a slight increased importance of the left medial temporal lobe. In other disease entities such as MTL sclerosis where left-right differences are key, this asymmetric distortion could be catastrophic for lesion detectability. The study utilized FSL/FLIRT for motion correction and eddy current compensation without description of b-matrix correction. The number of diffusion directions was 32 with a b-value of 1200, and the NEX was very high at 12. This study is the first of its kind to push resolution with the aim of perforant pathway imaging, but SNR is admittedly low given the resolution.

Finally, a recent investigation utilizing diffusion spectrum imaging is of interest and the first of its kind with regard to the MTL. Six volunteers were scanned with 2.2 × 2.2 × 3.0 mm resolution, GRAPPA 2, b=8000 (presumably with the use of insert gradients though this was not described), 258 directions, one b=0 image. Diffusion spectrum processing was performed, and their figures demonstrate reconstruction of the hippocampal-fornix output path to the mammillary bodies, as well as the parahippocampal cingulum bundle. While interesting, tractography of the fornix can be accomplished with conventional tractography and quicker data acquisitions on conventional scanners [66] (Figure 9). Crossing fiber resolved methods such as this will surely be a subject of future studies.

**Ex vivo—**A 7T study on hippocampal diffusion demonstrated variations in anisotropy and orientation throughout the hippocampal subfields [67]. Another study by the same author demonstrated further details in the rat hippocampus including the rat perforant pathway [68].

A very impressive detailed tractography analysis of the MTL has recently been published [69]. At 4.7T, specimens were imaged for 40 hours to achieve 200 μm isotropic data at a b-value of 4000 with 20 directions at a TE of 28 using a 3D sequence. Tractography was performed deterministically with DTI Studio and probabilistically with eddy current correction using FSL's Diffusion Toolbox. Using either method, tracts were observed extending from the entorhinal cortex to the subiculum, and then from the subiculum to the CA fields and dentate gyrus. The subiculum was effectively a waypoint: all tractography stopped at this waypoint, and neither algorithm would trace directly from the entorhinal

cortex to the CA fields/dentate gyrus. This landmark study is the first of its kind to demonstrate known pathways on a microscopic level.

## Future Directions

Performing high quality diffusion tensor imaging in an elderly patient population presents a technical challenge, and all of the papers cited in this study are of merit. Several points are obvious from this paper to direct future endeavors. First, there is marked inconsistency in the literature with regard to MR methodology. None of the *in vivo* study examined in this paper described utilization of parallel imaging, eddy current compensation, motion correction, and b-matrix correction simultaneously. These are all tools available on all scanning platforms and with free software, so all future studies should employ these methods.

A second point is regarding resolution. The resolution of a study needs to support the claims. Microstructure requires small pixels, volumetrically. Furthermore, all of the tractography programs have been developed with isotropic imaging to avoid directional bias. To advance the field, future work needs to pursue high-resolution isotropic imaging with low distortion. None of the listed studies offered a measurement of the SNR of their images. While it is difficult to measure the SNR of diffusion weighted images, one can easily measure the SNR of the b=0 image with several repetitions; this only adds one minute at most to a sequence. Reporting this number will enable the scientific community to understand another source of variance.

Some newer methods of diffusion-weighted acquisition may provide a better balance of SNR and voxel size such as 3D balanced steady state free precession imaging [70]. It is unclear if methodologies relying on the orientation of white matter with respect to the main magnetic field will prove to be applicable [71, 72, 73].

Diffusion tensor imaging on specimens will help validate claims made by tractography, especially with the advance of methods that resolve crossing fibers. However, one needs to be cognizant of the limitations associated with fixed brains (e.g. biological decay, volume change, significantly higher b-value required, diffusion in blood vessels that contain flowing blood *in vivo* but *ex vivo* may have measurable diffusion characteristics, and larger susceptibility artifacts). Polarized light microscopy may help verify the results of tractography [74].

## Impact for Clinical and Research Diffusion Studies of the MTL

This paper suggests that future research studies and clinical work of the MTL, including AD and epilepsy, should adhere to the following guidelines.

Acquisition:

- 3T imaging is preferable over 1.5T
- Axial plane imaging with 2.0mm isotropic voxels with the phase-encode axis A-P
    - ○ To minimize partial voluming and keep distortions L-R symmetric
    - ○ Coronal plane imaging can be pursued with anisotropic voxels, but caution should be exercised regarding distortions and bias in tractography
- High-order shimming to include at least second-order terms
    - ○ To reduce B0 inhomogeneity and associated image distortion

- Eddy current compensation either with twice-refocused diffusion preparation (dual spin echo) and/or correction using post-processing
    - To reduce eddy current artifacts
- Motion correction and b-matrix correction
    - Reduce the effect of motion and secondary effects of rotation on the direction of the encoding gradients. This may not necessarily be readily available clinically, but perhaps vendors will develop such tools
    - Visually exam (or use software) to exclude slices with severe signal drop outs due to patient motion or brain pulsation – peripheral gating can mitigate image quality but prolongs scan time, which is prohibitive in AD patients.
- At least 30 diffusion directions for DTI [75][61]
- SNR measurement
    - Will facilitate standardization and the interpretation of differences among research studies

Processing:

- Segmentation of MTL structures
    - Either performed on or coregistered to the b = 0 images to ensure no misalignment
- Subregion analysis
    - Should refer to standard atlases [9]
- Measurement of both FA and MD

## Acknowledgments

Sources of Support: RSNA Research and Education Foundation Research Fellow Award General Electric National Institutes of Health

## References

1. Lewis FT. The Significance of the Term Hippocampus. The Journal of Comparative Neurology. April; 1923 35(3):213–30.
2. Walther C. Hippocampal terminology: concepts, misconceptions, origins. Endeavour. Jun; 2002 26(2):41–4. [PubMed: 12174467]
3. Papez JW. A Proposed Mechanism of Emotion. Archives of Neurology and Psychiatry. 1937; 38:725–33.
4. SCOVILLE WB, MILNER B. Loss of recent memory after bilateral hippocampal lesions. J Neurol Neurosurg Psychiatry. Feb; 1957 20(1):11–21. [PubMed: 13406589]
5. Milner B, Corkin S, Teuber HL. Further Analysis of the Hippocampal Amnesic Syndrome: 14-Year Follow-Up Study of H.M. Neuropsychologia. 1968; 6:215–34.
6. Aggleton JP, Brown MW. Episodic memory, amnesia, and the hippocampal-anterior thalamic axis. Behav Brain Sci. Jun; 1999 22(3):425–44. discussion 444-89. [PubMed: 11301518]
7. Nieuwenhuys, R.; Voogd, J.; Van Huijzen, C., et al. The human central nervous system. Springer Verlag; 2008.
8. Duvernoy, HM. The human hippocampus: functional anatomy, vascularization, and serial sections with MRI. Springer Verlag; 2005.
9. Insausti, R.; Amaral, DG. The Human Nervous System, Second Edition: Hippocampal Formation. 2nd edition. Paxinos, G.; Mai, JK., editors. Academic Press; 2004. p. 871-914.

10. Suzuki WA, Amaral DG. Topographic organization of the reciprocal connections between the monkey entorhinal cortex and the perirhinal and parahippocampal cortices. J Neurosci. Mar; 1994 14(3 Pt 2):1856–77. [PubMed: 8126576]
11. Witter MP, Amaral DG. Entorhinal cortex of the monkey: V. Projections to the dentate gyrus, hippocampus, and subicular complex. J Comp Neurol. May; 1991 307(3):437–59. [PubMed: 1713237]
12. Mufson EJ, Brady DR, Kordower JH. Tracing neuronal connections in postmortem human hippocampal complex with the carbocyanine dye DiI. Neurobiol Aging. 1990; 11(6):649–53. [PubMed: 1704107]
13. Hevner RF, Kinney HC. Reciprocal entorhinal-hippocampal connections established by human fetal midgestation. J Comp Neurol. Aug; 1996 372(3):384–94. [PubMed: 8873867]
14. Braak H, Braak E. Neuropathological stageing of Alzheimer-related changes. Acta Neuropathol. 1991; 82(4):239–259. [PubMed: 1759558]
15. Mirra SS, Heyman A, McKeel D, et al. The Consortium to Establish a Registry for Alzheimer's Disease (CERAD). Part II. Standardization of the neuropathologic assessment of Alzheimer's disease. Neurology. Apr; 1991 41(4):479–86. [PubMed: 2011243]
16. Trojanowski JQ, Lee VMY. The role of tau in Alzheimer's disease. Med Clin North Am. May; 2002 86(3):615–27. [PubMed: 12168561]
17. Giannakopoulos P, Kövari E, Gold G, et al. Pathological substrates of cognitive decline in Alzheimer's disease. Front Neurol Neurosci. 2009; 24:20–9. [PubMed: 19182459]
18. Gómez-Isla T, Hollister R, West H, et al. Neuronal loss correlates with but exceeds neurofibrillary tangles in Alzheimer's disease. Ann Neurol. Jan; 1997 41(1):17–24. [PubMed: 9005861]
19. Vemuri P, Wiste HJ, Weigand SD, et al. MRI and CSF biomarkers in normal, MCI, and AD subjects: predicting future clinical change. Neurology. Jul; 2009 73(4):294–301. [PubMed: 19636049]
20. Lehéricy S, Marjanska M, Mesrob L, et al. Magnetic resonance imaging of Alzheimer's disease. Eur Radiol. Feb; 2007 17(2):347–62. [PubMed: 16865367]
21. Bookheimer SY, Strojwas MH, Cohen MS, et al. Patterns of brain activation in people at risk for Alzheimer's disease. N Engl J Med. Aug; 2000 343(7):450–6. [PubMed: 10944562]
22. Bookheimer S, Burggren A. APOE-4 genotype and neurophysiological vulnerability to Alzheimer's and cognitive aging. Annu Rev Clin Psychol. 2009; 5:343–62. [PubMed: 19327032]
23. Greicius MD, Srivastava G, Reiss AL, et al. Default-mode network activity distinguishes Alzheimer's disease from healthy aging: evidence from functional MRI. Proc Natl Acad Sci U S A. Mar; 2004 101(13):4637–42. [PubMed: 15070770]
24. Hess CP. Update on diffusion tensor imaging in Alzheimer's disease. Magn Reson Imaging Clin N Am. May; 2009 17(2):215–24. [PubMed: 19406355]
25. Jack CR Jr, Knopman DS, Jagust WJ, et al. Hypothetical model of dynamic biomarkers of the Alzheimer's pathological cascade. Lancet Neurol. Jan; 2010 9(1):119–28. [PubMed: 20083042]
26. Klunk WE, Engler H, Nordberg A, et al. Imaging brain amyloid in Alzheimer's disease with Pittsburgh Compound-B. Ann Neurol. Mar; 2004 55(3):306–19. [PubMed: 14991808]
27. Bacskai BJ, Frosch MP, Freeman SH, et al. Molecular imaging with Pittsburgh Compound B confirmed at autopsy: a case report. Arch Neurol. Mar; 2007 64(3):431–4. [PubMed: 17353389]
28. Gómez-Isla T, Price JL, McKeel DW Jr, et al. Profound loss of layer II entorhinal cortex neurons occurs in very mild Alzheimer's disease. J Neurosci. Jul; 1996 16(14):4491–500. [PubMed: 8699259]
29. Hyman BT, Van Hoesen GW, Damasio AR, et al. Alzheimer's disease: cell-specific pathology isolates the hippocampal formation. Science. Sep; 1984 225(4667):1168–70. [PubMed: 6474172]
30. Van Hoesen GW, Hyman BT, Damasio AR. Entorhinal cortex pathology in Alzheimer's disease. Hippocampus. Jan; 1991 1(1):1–8. [PubMed: 1669339]
31. Beaulieu C. The basis of anisotropic water diffusion in the nervous system - a technical review. NMR Biomed. 2002; 15(7-8):435–55. [PubMed: 12489094]

32. Kantarci K, Avula R, Senjem ML, et al. Dementia with Lewy bodies and Alzheimer disease: neurodegenerative patterns characterized by DTI. Neurology. Jun; 2010 74(22):1814–21. [PubMed: 20513818]
33. Sexton CE, Kalu UG, Filippini N, et al. A meta-analysis of diffusion tensor imaging in mild cognitive impairment and Alzheimer's disease. Neurobiol Aging. Jul.2010
34. Hong YJ, Yoon B, Shim YS, et al. Differences in microstructural alterations of the hippocampus in Alzheimer disease and idiopathic normal pressure hydrocephalus: a diffusion tensor imaging study. AJNR Am J Neuroradiol. Nov; 2010 31(10):1867–72. [PubMed: 20671063]
35. Salat DH, Tuch DS, van der Kouwe AJW, et al. White matter pathology isolates the hippocampal formation in Alzheimer's disease. Neurobiol Aging. Feb; 2010 31(2):244–56. [PubMed: 18455835]
36. Zhang Y, Schuff N, Jahng G, et al. Diffusion tensor imaging of cingulum fibers in mild cognitive impairment and Alzheimer disease. Neurology. Jan; 2007 68(1):13–9. [PubMed: 17200485]
37. Rose SE, McMahon KL, Janke AL, et al. Diffusion indices on magnetic resonance imaging and neuropsychological performance in amnestic mild cognitive impairment. J Neurol Neurosurg Psychiatry. Oct; 2006 77(10):1122–8. [PubMed: 16754694]
38. Müller MJ, Greverus D, Dellani PR, et al. Functional implications of hippocampal volume and diffusivity in mild cognitive impairment. Neuroimage. Dec; 2005 28(4):1033–42. [PubMed: 16084115]
39. Fellgiebel A, Wille P, Müller MJ, et al. Ultrastructural hippocampal and white matter alterations in mild cognitive impairment: a diffusion tensor imaging study. Dement Geriatr Cogn Disord. 2004; 18(1):101–8. [PubMed: 15087585]
40. Rogalski EJ, Murphy CM, deToledo-Morrell L, et al. Changes in parahippocampal white matter integrity in amnestic mild cognitive impairment: a diffusion tensor imaging study. Behav Neurol. 2009; 21(1):51–61. [PubMed: 19847045]
41. Choo IH, Lee DY, Oh JS, et al. Posterior cingulate cortex atrophy and regional cingulum disruption in mild cognitive impairment and Alzheimer's disease. Neurobiol Aging. May; 2010 31(5):772–9. [PubMed: 18687503]
42. Yakushev I, Gerhard A, Müller MJ, et al. Relationships between hippocampal microstructure, metabolism, and function in early Alzheimer's disease. Brain Struct Funct. Feb.2011
43. Chua TC, Wen W, Slavin MJ, et al. Diffusion tensor imaging in mild cognitive impairment and Alzheimer's disease: a review. Curr Opin Neurol. Feb; 2008 21(1):83–92. [PubMed: 18180656]
44. Stebbins GT, Murphy CM. Diffusion tensor imaging in Alzheimer's disease and mild cognitive impairment. Behav Neurol. 2009; 21(1):39–49. [PubMed: 19847044]
45. Jones DK, Leemans A. Diffusion tensor imaging. Methods Mol Biol. 2011; 711:127–44. [PubMed: 21279600]
46. Jones DK, Cercignani M. Twenty-five pitfalls in the analysis of diffusion MRI data. NMR Biomed. Aug; 2010 23(7):803–20. [PubMed: 20886566]
47. Embleton KV, Haroon HA, Morris DM, et al. Distortion correction for diffusion-weighted MRI tractography and fMRI in the temporal lobes. Hum Brain Mapp. Oct; 2010 31(10):1570–87. [PubMed: 20143387]
48. von Morze C, Kelley DAC, Shepherd TM, et al. Reduced field-of-view diffusion-weighted imaging of the brain at 7 T. Magn Reson Imaging. Dec; 2010 28(10):1541–5. [PubMed: 20850242]
49. Kim D, Adalsteinsson E, Glover GH, et al. Regularized higher-order in vivo shimming. Magn Reson Med. Oct; 2002 48(4):715–22. [PubMed: 12353290]
50. Reese TG, Heid O, Weisskoff RM, et al. Reduction of eddy-current-induced distortion in diffusion MRI using a twice-refocused spin echo. Magn Reson Med. Jan; 2003 49(1):177–82. [PubMed: 12509835]
51. Rohde GK, Barnett AS, Basser PJ, et al. Comprehensive approach for correction of motion and distortion in diffusion-weighted MRI. Magn Reson Med. Jan; 2004 51(1):103–14. [PubMed: 14705050]

52. Andersson JLR, Skare S. A model-based method for retrospective correction of geometric distortions in diffusion-weighted EPI. Neuroimage. May; 2002 16(1):177–99. [PubMed: 11969328]
53. Haselgrove JC, Moore JR. Correction for distortion of echo-planar images used to calculate the apparent diffusion coefficient. Magn Reson Med. Dec; 1996 36(6):960–4. [PubMed: 8946363]
54. Frank LR. Anisotropy in high angular resolution diffusion-weighted MRI. Magn Reson Med. Jun; 2001 45(6):935–9. [PubMed: 11378869]
55. Frank LR. Characterization of anisotropy in high angular resolution diffusion-weighted MRI. Magn Reson Med. Jun; 2002 47(6):1083–99. [PubMed: 12111955]
56. Wedeen VJ, Wang RP, Schmahmann JD, et al. Diffusion spectrum magnetic resonance imaging (DSI) tractography of crossing fibers. Neuroimage. Jul; 2008 41(4):1267–77. [PubMed: 18495497]
57. Wedeen VJ, Hagmann P, Tseng WI, et al. Mapping complex tissue architecture with diffusion spectrum magnetic resonance imaging. Magn Reson Med. Dec; 2005 54(6):1377–86. [PubMed: 16247738]
58. Tuch DS. Q-ball imaging. Magn Reson Med. Dec; 2004 52(6):1358–72. [PubMed: 15562495]
59. Tournier J, Yeh C, Calamante F, et al. Resolving crossing fibres using constrained spherical deconvolution: validation using diffusion-weighted imaging phantom data. Neuroimage. Aug; 2008 42(2):617–25. [PubMed: 18583153]
60. Alexander DC. Maximum entropy spherical deconvolution for diffusion MRI. Inf Process Med Imaging. 2005; 19:76–87. [PubMed: 17354686]
61. Jones DK. The effect of gradient sampling schemes on measures derived from diffusion tensor MRI: a Monte Carlo study. Magn Reson Med. Apr; 2004 51(4):807–15. [PubMed: 15065255]
62. Kalus P, Slotboom J, Gallinat J, et al. Examining the gateway to the limbic system with diffusion tensor imaging: the perforant pathway in dementia. Neuroimage. Apr; 2006 30(3):713–20. [PubMed: 16337815]
63. Mielke MM, Kozauer NA, Chan KCG, et al. Regionally-specific diffusion tensor imaging in mild cognitive impairment and Alzheimer's disease. Neuroimage. May; 2009 46(1):47–55. [PubMed: 19457371]
64. Salmenpera TM, Simister RJ, Bartlett P, et al. High-resolution diffusion tensor imaging of the hippocampus in temporal lobe epilepsy. Epilepsy Res. Oct; 2006 71(2-3):102–6. [PubMed: 16870399]
65. Yassa MA, Muftuler LT, Stark CEL. Ultrahigh-resolution microstructural diffusion tensor imaging reveals perforant path degradation in aged humans in vivo. Proc Natl Acad Sci U S A. Jul; 2010 107(28):12687–91. [PubMed: 20616040]
66. Concha L, Livy DJ, Beaulieu C, et al. In vivo diffusion tensor imaging and histopathology of the fimbria-fornix in temporal lobe epilepsy. J Neurosci. Jan; 2010 30(3):996–1002. [PubMed: 20089908]
67. Shepherd TM, Ozarslan E, Yachnis AT, et al. Diffusion tensor microscopy indicates the cytoarchitectural basis for diffusion anisotropy in the human hippocampus. AJNR Am J Neuroradiol. May; 2007 28(5):958–64. [PubMed: 17494678]
68. Shepherd TM, Ozarslan E, King MA, et al. Structural insights from high-resolution diffusion tensor imaging and tractography of the isolated rat hippocampus. Neuroimage. Oct; 2006 32(4): 1499–509. [PubMed: 16806988]
69. Augustinack JC, Helmer K, Huber KE, et al. Direct visualization of the perforant pathway in the human brain with ex vivo diffusion tensor imaging. Front Hum Neurosci. 2010; 4:42. [PubMed: 20577631]
70. McNab JA, Miller KL. Steady-state diffusion-weighted imaging: theory, acquisition and analysis. NMR Biomed. Aug; 2010 23(7):781–93. [PubMed: 20886565]
71. Liu, C. Susceptibility Tensor Imaging.. Proceedings of the ISMRM. 2010.
72. Miller KL, Smith SM, Jezzard P. Asymmetries of the balanced SSFP profile. Part II: white matter. Magn Reson Med. Feb; 2010 63(2):396–406. [PubMed: 20099329]
73. Miller KL. Asymmetries of the balanced SSFP profile. Part I: theory and observation. Magn Reson Med. Feb; 2010 63(2):385–95. [PubMed: 20099328]

74. Axer M, Amunts K, Grässel D, et al. A novel approach to the human connectome: ultra-high resolution mapping of fiber tracts in the brain. Neuroimage. Jan; 2011 54(2):1091–101. [PubMed: 20832489]

75. Skare S, Hedehus M, Moseley ME, et al. Condition number as a measure of noise performance of diffusion tensor data acquisition schemes with MRI. J Magn Reson. Dec; 2000 147(2):340–52. [PubMed: 11097823]

76. Alexander DC, Pierpaoli C, Basser PJ, et al. Spatial transformations of diffusion tensor magnetic resonance images. IEEE Trans Med Imaging. Nov; 2001 20(11):1131–9. [PubMed: 11700739]

77. Woods RP, Grafton ST, Holmes CJ, et al. Automated image registration: I. General methods and intrasubject, intramodality validation. J Comput Assist Tomogr. 1998; 22(1):139–52. [PubMed: 9448779]

78. Zeineh MM, Engel SA, Thompson PM, et al. Unfolding the human hippocampus with high resolution structural and functional MRI. Anat Rec. Apr; 2001 265(2):111–20. [PubMed: 11323773]

79. Cook, P.; Bai, Y.; Nedjati-Gilani, S.; Seunarine, K.; Hall, M.; Parker, G.; Alexander, D. Camino: Open-source diffusion-MRI reconstruction and processing.. 14th Scientific Meeting of the International Society for Magnetic Resonance in Medicine; 2006.

80. Basser PJ, Mattiello J, LeBihan D. Estimation of the effective self-diffusion tensor from the NMR spin echo. J Magn Reson B. Mar; 1994 103(3):247–54. [PubMed: 8019776]

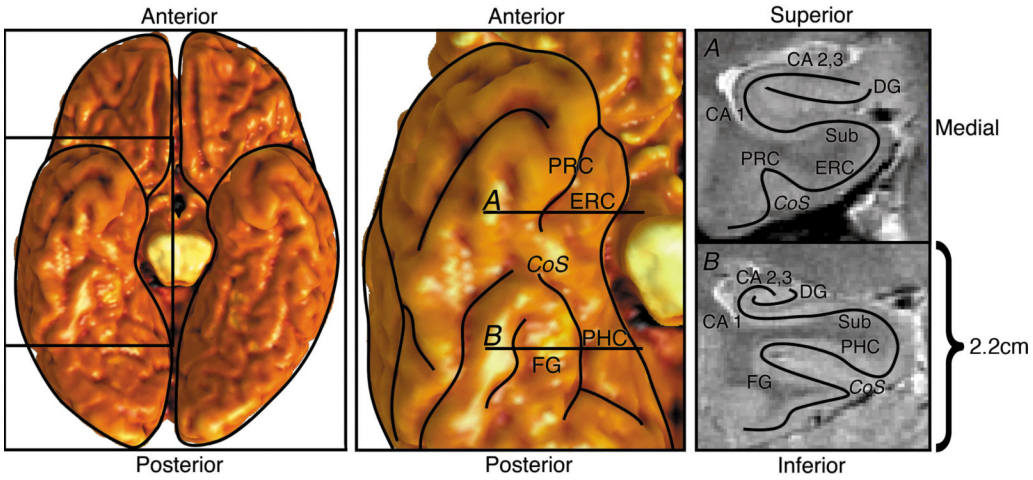


**Figure 1.**

Anatomical diagram, with an inferior view of the temporal lobe at the left, and coronal sections from the two indicated slices at the right. A: Anterior slice through entorhinal cortex. B: Posterior slice through parahippocampal cortex. ERC, entorhinal cortex; PRC, perirhinal cortex; PHC, parahippocampal cortex; FG, fusiform gyrus; Sub, subiculum; CA 1, cornu ammonis 1; CA 2,3, CA fields 2 and 3; DG, dentate gyrus; CoS, collateral sulcus (Reproduced in black and white from [78], adding a scale bar).

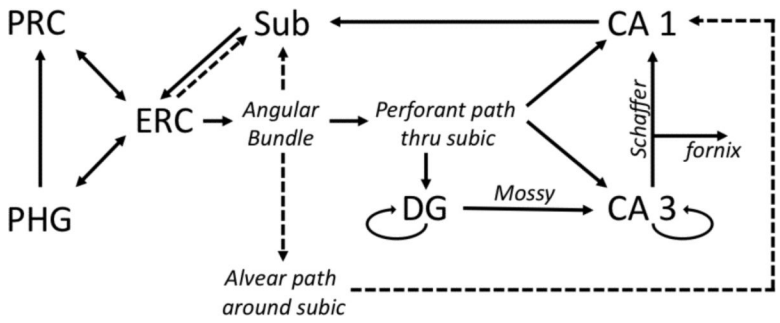


**Figure 2.**
Pathways of the medial temporal lobe. Solid lines indicate major pathways, and dotted lines are minor pathways. For abbreviations, please see the legend to Figure 1.

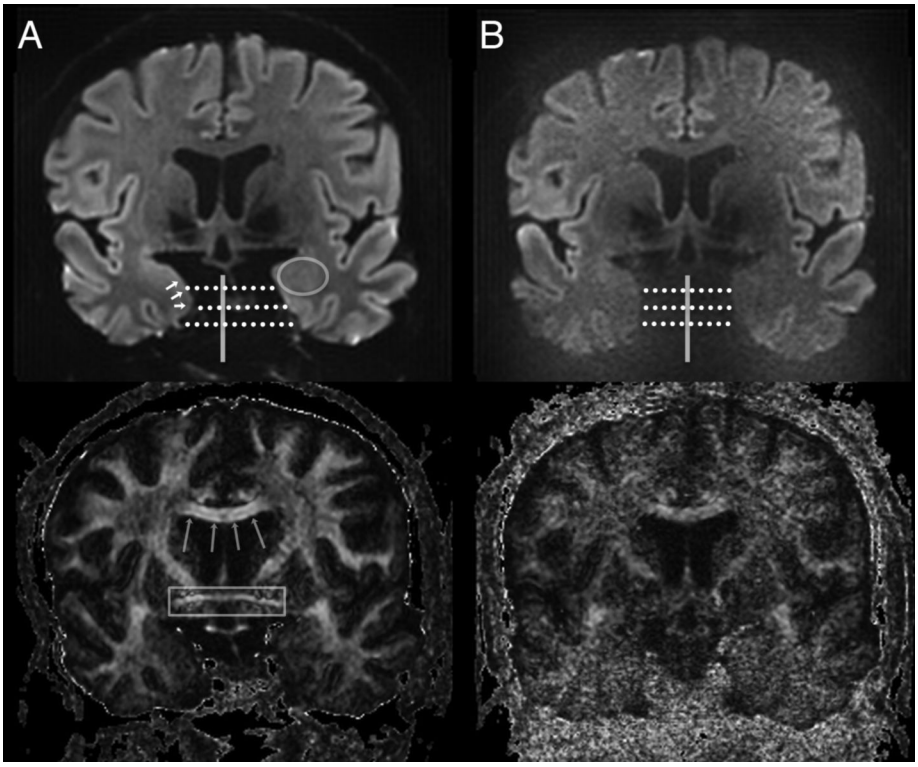


**Figure 3.**
Coronal 3mm thick 1.2 mm in plane diffusion weighted EPI image at the anterior level of the anterior medial temporal lobe. A circle surrounds the left amygdala. Short arrows outline the approximate location of the right entorhinal cortex. Long arrows define the corpus callosum, and a box surrounds the anterior commissure. (A: Left column) Phase-encode left-right with diffusion weighted image at the top and FA on bottom. This demonstrates asymmetric distortion along the left-right axis. (B: Right column) Phase-encode supero-inferior demonstrates left-right symmetry, but severe noise because of inadequate coil separation to support parallel imaging along this axis.

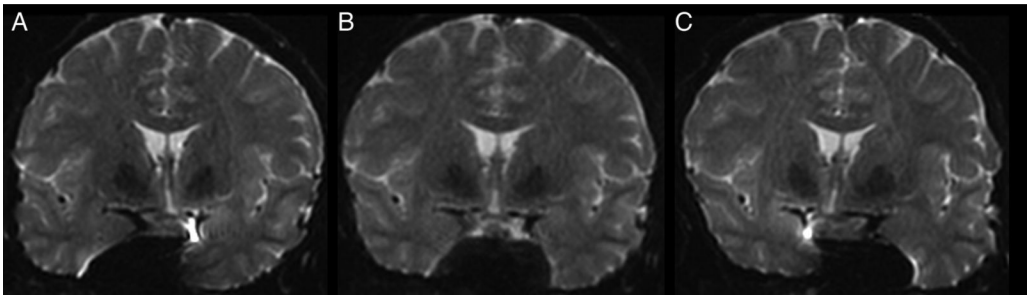


**Figure 4.**
Coronal image (A) phase-encode traversal in one direction and (B) phase-encode traversal in the opposite direction. After correction (C), distortion is significantly reduced at the cost of minor blurring.

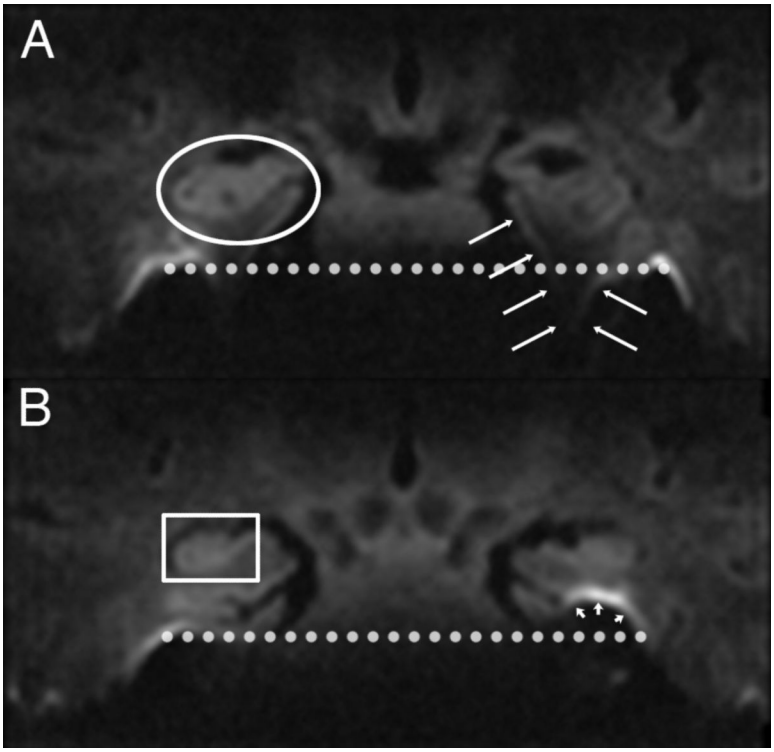


**Figure 5.**
Zoom EPI Direct Coronal Acquisition. A) Anterior section. The right hippocampal head is circled. The left parahippocampal gyrus is outlined by arrows. Note distortion is present with inferior pointing of both parahippocampal gyri, but it is left-right symmetric (note the dotted horizontal line). B) Posterior Section. The right hippocampal body is within the square. Because of differential pneumatization of the petrous apices, distortion is asymmetrically worse on the left parahippocampal gyrus (arrowheads) compared to the right, even though the phase-encode axis is supero-inferior.

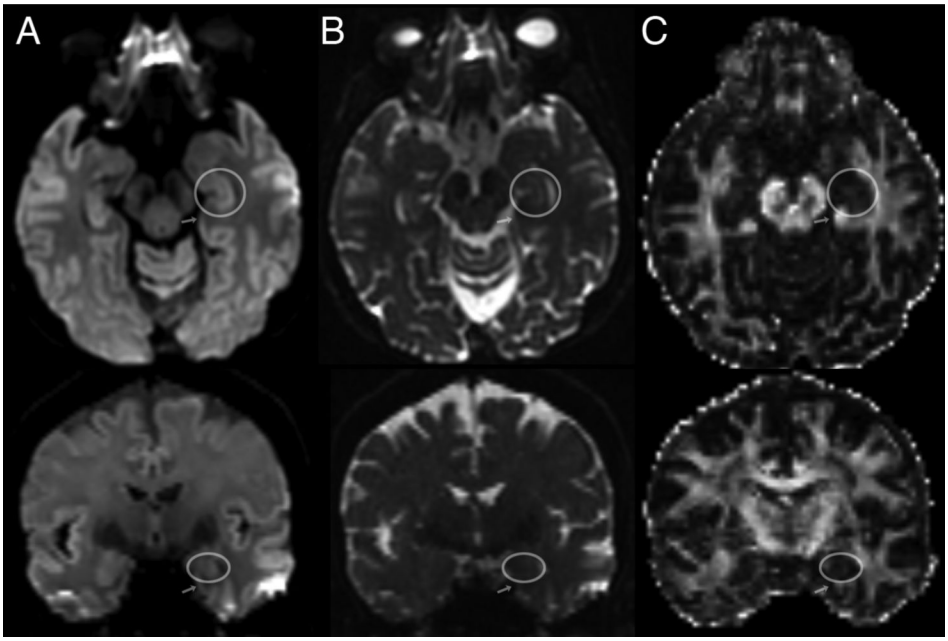


**Figure 6.**
Top row: axial diffusion (A) weighted EPI 2mm isotropic resolution, T2-weighted EPI (B), and FA map (C) at 3T with the phase encode axis A-P. The left hippocampal head and amygdala are outlined by the circle, and an arrow points to the left parahippocampal gyrus (anterior parahippocampal gyrus on the coronal images, mid parahippocampal gyrus in the axial plane). These images demonstrate symmetric left-right distortion. Coronal reformats (bottom row) have inferior definition of medial temporal microstructure compared to anisotropic coronal acquisitions (Figure 3A, 5, and 8) but demonstrate relatively symmetric distortion.

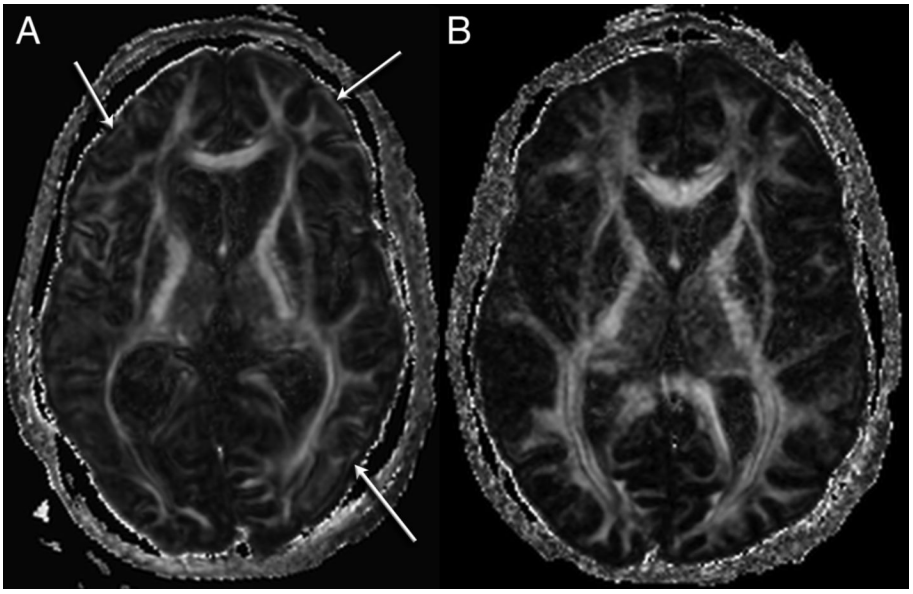


**Figure 7.**

A) Single refocused spin echo has better SNR but artificial FA at the cortices and edges of the image (arrows). B) Twice refocused (on a different subject) has less SNR but less cortical FA artifact. Acquisitions are matched for imaging time.

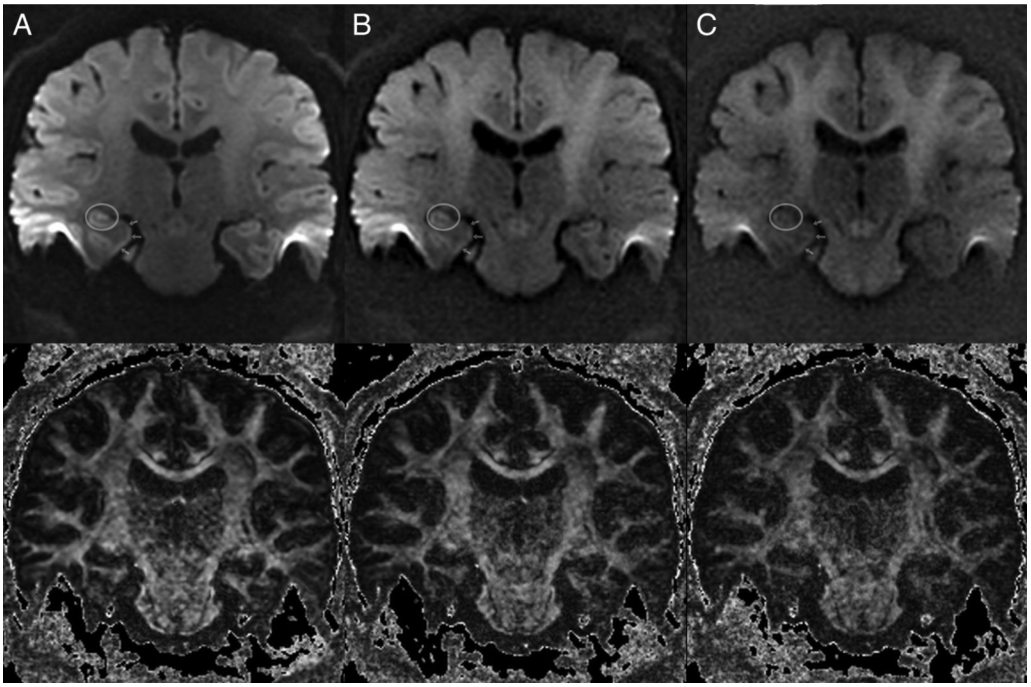


**Figure 8.**
Coronal diffusion weighted images (top) and FA maps for (A) b = 1000, (B) b = 2000, and (C) b = 3000. The right hippocampal body is encircled, and arrows outline the right parahippocampal gyrus. SNR progressively declines as the b-value increases.

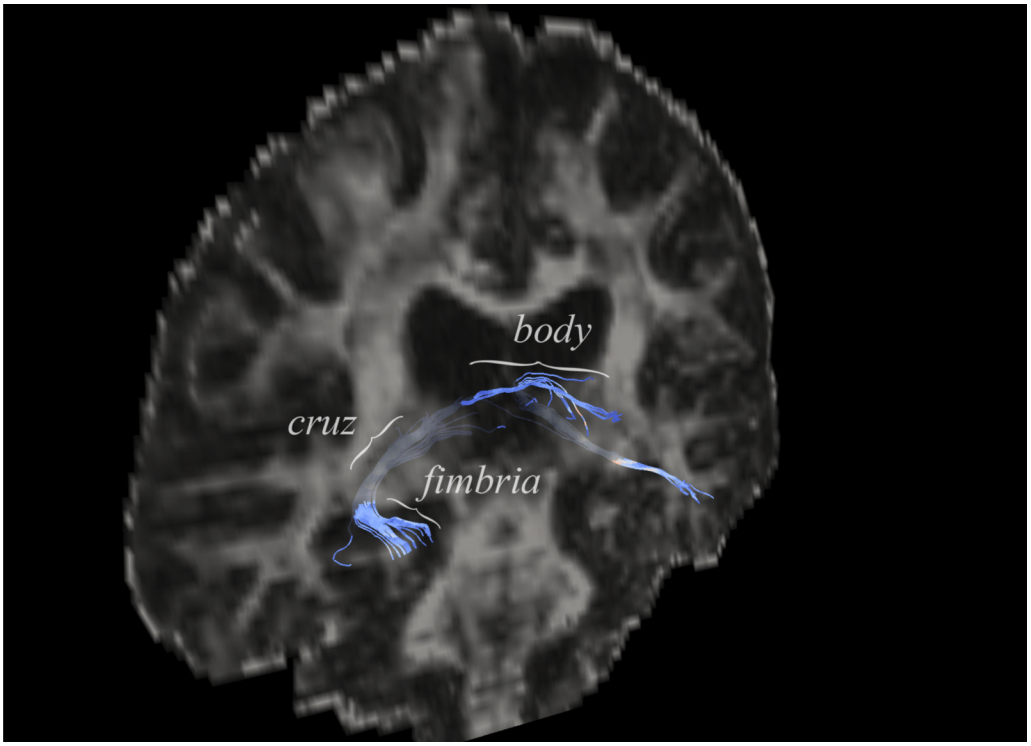


**Figure 9.**
Tractography of the fornix. A whole brain b2000 dataset at 3.0T with 2mm isotropic acquisition and 40 directions, processed with conventional DTI analysis using Camino, displayed with Paraview. ROIs were selected along the fornix with a waypoint in the fimbria of the fornix along the superior hippocampal body. An exclusion ROI was selected in the anterior hippocampal head. The fimbria, cruz, and body of the right fornix are labeled. [79, 80]

**Table 1**

ults Across Studies.

| C | Field Strength | Voxel Size | B-Value | TE | Diffusion Directions - # B0 images, NEX | Parallel Imaging | Eddy Current Compensation or Correction | Motion Correction | B Matrix Correction | Other | Analysis | Significant Results |
|---|---|---|---|---|---|---|---|---|---|---|---|---|
| | 1.5 | × - × 5 | 900 | 100 | 6/1/1 | N | N | N | N | | ROI: FA/MD | L HC MD: AD>MCI>NC<br>L HC FA: NC > MCI = AD |
| | 1.5 | 1.8 × 1.8 × 3.0 | 900 | 100 | 6/1/1 | N | N | N | N | | ROI: FA/MD | B HC MD: MCI > NC<br>B HC FA: NC > MCI |
| | 1.5 | 1.8 × 1.8 × 2.8 | 1100 | 106 | 44/16/1 | N | N | N | N | | VBA: FA/MD | B ERC MD: MCI > NC<br>B Limbic FA: MCI < NC |
| | 1.5 | 2.3 × 2.5 × 2.5 | 1200 | 87 | 6/1/1 | N | Dual Echo | Y | -[1] | | ROI: Intervoxel Coherence | B HC, ERC, and PPZ Intervoxel Coherence: NC > MCI > NC |
| | 1.5 | 2.3 × 2.3 × 3.0 | 1000 | 100 | 6/1/1 | N | - | N | N | FLAIR | ROI: FA/MD | B HC MD: AD>NC (MCI NS)<br>B HC FA: NC > MCI = AD |
| | 1.5 | 2.0 × 2.0 × 2.0 | 700 | 89 | 60/10/1 | N | Dual Echo | FLIRT | -[2] | | TBSS FA/MD, FA along PHG track | B MTL FA: NC>AD<br>B MTL MD: AD>NC<br>B PHG Tract Based FA: NC>AD |
| | 3.0 | 2.2 × 2.2 × 2.2 | 700 | 80 | 32/5/2 | SENSE 2.5 | AIR | AIR | N | B33 instead of B0 | ROI:FA | Fornix FA: NC=MCI>AD<br>NS MTL differences between AD, MCI, and NC |
| | 1.5 | 2.0 × 2.0 × 3.0 | 800 | 97 | 24/1/6 | N | Rohde | Rohde | Y | | ROI: FA/MD, FA/MD along PHG track | B PHG FA: NS difference<br>B PHG MD: MCI>NC<br>B PHG Tract based FA: NS<br>B PHG Tract based MD: MCI>NC |

| C | Field Strength | Voxel Size | B-Value | TE | Diffusion Directions - # B0 images, NEX | Parallel Imaging | Eddy Current Compensation or Correction | Motion Correction | B Matrix Correction | Other | Analysis | Significant Results |
|---|---|---|---|---|---|---|---|---|---|---|---|---|
| | 3.0 | 1.8 × 1.8 × 3.5 | 1000 | 77 | 25/1/1 | N | Dual Echo | N | N | | ROI: FA/MD | L PHG FA: NC>AD=MCI<br>R PHG FA: NC>AD (MCI NS)<br>B PHG MD: NS |
| | 3T | × 3 × 3.3 | 1000 | 60 | 21/1/1 | ASSET 2 | AIR | AIR | N | FLAIR | VBA on MD (ROI based FA did not include the MTL) | B HC/PHG MD: AD>NC |
| | 1.5 | .0 × 2.0 × 4.0 | 1000 | 83 | 25/1/1 | N | N | N | N | | ROI: FA/MD | B HC MD: AD>NC<br>B HC FA: NC>AD |
| | 1.5 | .8 × 1.8 × 3.0 | 1000 | 105 | 6/1/6 | GRAPPA | N | Manual exclusion of motion laden scans | N | FDG-PET also obtained | ROI: MD | L HC MD correlates inversely with FDG-PET and delayed verbal recall |

upplied in the paper. NEX was assumed to be 1 if it was not listed. Similarly, the number of b=0 images was also assumed to be 1 if not listed.

ed Image Registration [77], ERC = Entorhinal Cortex, FA = Fractional Anisotropy, GRAPPA = Gene- Ralized Autocalibrating Partially Parallel Acquisitions, mentia, MD = Mean Diffusivity, NC = Normal Control, NPH = Normal Pressure Hydrocephalus, NS = No Significant, PPZ = Perforant Pathway Zone, Rohde =

sation is cited in the eddy correction methods, but this method applies to rotating the tensor, not rotating the raw diffusion images [76].

fter motion correction, but this paper did not cite use of this compensation.

*Top Magn Reson Imaging*. Author manuscript; available in PMC 2011 December 15.